Measurement of Heat Release Rate, Aerosol, and Gas Products During Lithium-Ion Battery Thermal Runaway in Devices

John Easton[1] and Ya-Ting Liao[2]
Case Western Reserve University, Cleveland, OH, 44135

Rosa Padilla[3], Gordon Berger[4], and Jay Owens[5]
Universities Space Research Association, Cleveland, OH, 44135

Claire Fortenberry[6], David Urban[7], Daniel Dietrich[8], Thomas Miller[9], and Thomas DeMichael[10]
NASA Glenn Research Center, Cleveland, OH, 44135

Lithium-ion batteries power a large and increasing number and variety of electronic devices, hand tools, and larger machinery, including automobiles, inevitably finding use in crewed space missions. Under abusive use conditions or due to manufacturing defects, these batteries can experience thermal runaway, where the battery electrolyte reacts, generating heat, aerosol, toxic gas products, and potentially flames, posing a threat to the enclosed, recycled atmosphere of a space vehicle. Beginning an effort to quantify the effects of thermal runaway in a crewed vehicle or habitat, the authors built an enclosure and flow measurement system, capturing products to measure heat release rate, aerosol, and gas products evolving from thermal runaway. The scale of these current and future tests ranges from individual battery cells to laptop battery packs and full-sized laptop computers. An initial series of tests examined the burning rate of ethanol pool fires of two different sizes, simulating an individual battery cell fire and a battery pack fire, respectively. These results showed good agreement in heat release rate in comparison to a heat of combustion analysis, validating the apparatus. A second series of tests examined the thermal runaway of the two 2500 mAh battery cell types. These results quantified the heat release rate and gas products produced during the thermal runaway of the tested battery cells. It also showed different responses between different batteries in terms of aerosol production and heat release, showing the need to test specific battery components in terms of heat and products produced.

I. Introduction

Lithium-ion batteries (LIBs) are ubiquitous in modern terrestrial applications, powering varying devices including cellular phones, tablet and laptop computers, powered hand tools, and increasing in scale to automobiles and residential and industrial power storage. Many of these products and applications have or will find their way into space vehicles, including the International Space Station as well as planned missions to and beyond low Earth orbit. One potential danger of LIBs is thermal runaway (TR), where the battery fails with the constituents undergoing chemical reactions that generate heat, aerosol, toxic gas products, and flames or explosions, depending on the mechanism and circumstances of the event. While dangerous in normal applications, these effects pose particular dangers in the

[1] Senior Scientist, GEARS contract, 21000 Brookpark Road, Mail Stop 77-5.
[2] Associate Professor, Department of Mechanical and Aerospace Engineering, 10900 Euclid Avenue.
[3] Formerly Senior Scientist, GEARS contract, 21000 Brookpark Road, Mail Stop 77-5.
[4] Senior Scientist, GEARS contract, 21000 Brookpark Road, Mail Stop 77-5.
[5] Senior Systems Engineer, GEARS contract, 21000 Brookpark Road, Mail Stop 77-5.
[6] Aerospace Engineer, Low-Gravity Exploration Technology Branch, 21000 Brookpark Road, Mail Stop 77-5.
[7] Branch Chief, Low-Gravity Exploration Technology Branch, 21000 Brookpark Road, Mail Stop 77-5.
[8] Aerospace Engineer, Low-Gravity Exploration Technology Branch, 21000 Brookpark Road, Mail Stop 110-3.
[9] Battery Specialist, Photovoltaic and Electrochemical Systems Branch, 21000 Brookpark Road, Mail Stop 309-1.
[10] Aerospace Engineer, Exploration Systems Office, 21000 Brookpark Road, Mail Stop 162-7.

enclosed environment of a space vehicle or habitat, due to the limited ability to counter and manage the effects[1, 2]. The Saffire experiments[3] showed that for the combustion of cellulose and PMMA, the hazardous smoke products were a greater hazard than the heat release. For LIB's the relative hazard of the gaseous products and smoke can be expected to be even more important. Consequently this program is directed to assessing these products in a realistic scenario.

Previous work studying thermal runaway in LIBs is on a scale or performed in ways that make application to space vehicles difficult. Many of these studies examined smaller LIB cells[4-9]. Work with laptop battery packs measured heat release rate and production of hydrogen fluoride (HF), a toxic product, using both a Fourier transform infrared (FTIR) and aerosol chemical analysis[4]. This work used a 15 kW propane burner to drive the LIBs to and past thermal runaway[4], with the additional heating past thermal runaway not feasible for planned future work with TR in devices. Other work examined battery cells similar to those used in the present study but in much larger flow systems and with heating of the cells lasting longer than thermal runaway. They also examined the particles and aerosol generated, finding many particles smaller than 500 nm and chemistry indicative of toxic products, including HF[5, 6]. Other research used enclosed test chambers, limiting the amount of oxygen via room air to the battery in TR[7-9]. Some of the work also collected gas samples and absorbed chemicals in solution, leading to estimates of total products released but with no dynamic measurements[7]. Some studies[8] used an accelerating rate calorimeter, which slowly increases battery cell temperature to TR in an enclosed chamber. This again limits the amount of oxygen available during TR and allows for total product analysis, not as a function of time. An additional method of reaching TR is to overcharge the LIB. One such experiment[9] examined this method in a closed cell, taking samples of gas products. As these studies showed, the methods of performing the experiment, from initiating TR to the type of measurements made and facilities used, affect the results and applicability of the studies. One study[10] examined six different methods of initiating thermal runaway, with four different battery states of charge. The results showed that the initiation method was as impactful as the state of charge, and the different methods affected gas production rate, mass loss, and maximum temperature. For spacecraft vehicle applications, the methods used to study the battery must be reflective of the type of environment and method of inducing thermal runaway.

The present work documents the initial steps to study thermal runaway in lithium-ion battery powered devices, particularly tablet and laptop computers, and quantify the risks posed to crewed space vehicles and habitats. Ultimately, the project will examine the heat, gas products, and aerosol released not only from a battery pack containing lithium-ion battery cells, but also the propagation to and effects from burning the device that contains the battery pack in thermal runaway. This future work will also look at extinguishing and containment strategies as they are proposed for future crewed missions. To conduct these tests, the authors constructed a test enclosure continuously vented with room air which allows for the containment, capture, and measurement of TR products, with an orifice plate mass flow meter measuring the ventilation and product stream. Gas sensors measuring O_2, CO_2, and CO; thermocouples; video cameras; and aerosol measurement instruments measure the gas products and events during TR. The system uses oxygen consumption calorimetry to estimate the heat released during thermal runaway.

This paper specifically describes the new apparatus and results from early validation tests. The first set of validation tests consisted of estimating the heat release rate from two pools of ethanol with different diameter, comparing that to the estimate of heat release based on loss of mass and the heat of combustion. The two diameters approximate thermal runaway from different capacity cells, or one cell and one multi-cell pack. The second set of tests reported here look at the general phenomena, heat release, gas products, and aerosol from two cells, with similar capacity but different chemistry.

II. Hardware Description and Experimental Methods

The experiment has been designed to contain, capture, and vent the aerosol and gas products from a lithium-ion battery (LIB) in thermal runaway (TR). Measurement of the battery during TR provides insight into the heat released, particle size distribution, gas species, and general phenomena for individual cells, laptop computer battery packs, and full-sized laptop computers. Overall, the experiment consists of a smaller inner enclosure for the test article and experiment operation within a larger enclosure, both connected to room ventilation and drawing room air through the system. The inner enclosure vents through a measurement duct equipped with an orifice plate to measure the flow rate. A variety of sensors monitor the test article temperature, mass, and the surrounding environmental conditions; temperature, static pressure and pressure change in the measurement duct; oxygen, carbon dioxide, and carbon monoxide in the product stream; and aerosol particle size distribution. The design of the enclosure, flow measurement system, and gas measurement for oxygen consumption calorimetry is inspired by the design of commercial cone calorimeters. The inner enclosure for the test article, though, is much larger than the test stage and containment for a cone calorimeter. This is in anticipation of capturing and measuring much larger releases of gas, aerosol, and flames

then would be expected for a standard cone calorimeter, as well as the much larger test articles, tablet and laptop computers, anticipated in future work for this project which a commercial cone calorimeter would not accommodate. This section describes the experiment containment and flow measurement system (Section II.A.), and data measurements (Section II.B). It will then describe the oxygen consumption calorimetry used to estimate heat release rate (Section II.C.). The discussion will then focus on two experiment conditions. The first will focus on burning pools of ethanol to provide confidence in the system performance (Section II.D.). Comparison of the heat release results obtained from the flow measurement system and oxygen consumption calorimetry with results using the mass lost and heat of combustion provides confidence in the operation of the system and the analysis. The size of the ethanol pools approximates the expected size of single cell thermal runaway and the expected size of a battery pack or electronic device in thermal runaway. The second set of tests examine the thermal runaway of individual 2500 mAh LIB cells (Section II.E.). These tests will provide the heat release, gas products, aerosol, and phenomena expected of larger battery packs, validating the system performance in conditions expected from future, larger scale tests.

The choice to use a vented enclosure and oxygen consumption calorimetry is driven by planned tests, with the current tests reported here validating and demonstrating the initial capabilities of this system. The vented enclosure accommodates a wide range of battery pack and device capacities, from individual cells described here to larger battery packs and full-size devices planned for future work. The flow through system prevents oxygen depletion during tests with larger capacity batteries or packs, which could occur with closed, constant volume calorimeters. This system, with the inclusion of sampling ports as needed, is well-suited for dynamic gas species, aerosol, and heat release measurements. Future tests examining the use of fire extinguishers, safety bags, and other thermal runaway mitigation techniques may also be performed in this system, with the sensors, devices, and processes enabling evaluation of these techniques. These requirements recommend against other calorimetry techniques, particularly constant volume techniques. The larger scale and continuous flow of this system lends itself to the use of oxygen consumption calorimetry to estimate heat release. Recent work[11] has shown limitations of oxygen consumption calorimetry, particularly due to internal heating and oxygen release from a cell during thermal runaway. While the future work must account for these limitations, the overall goal of measuring impact to a vehicle environment and testing of runaway mitigation techniques limits the availability of other calorimetry techniques. This is particularly true for the future tests involving thermal runaway of battery packs still housed within a device, where the presence of the device can obscure the confounding effects, and the calorimetry must also account for any subsequent ignition of the device triggered by the thermal runaway.

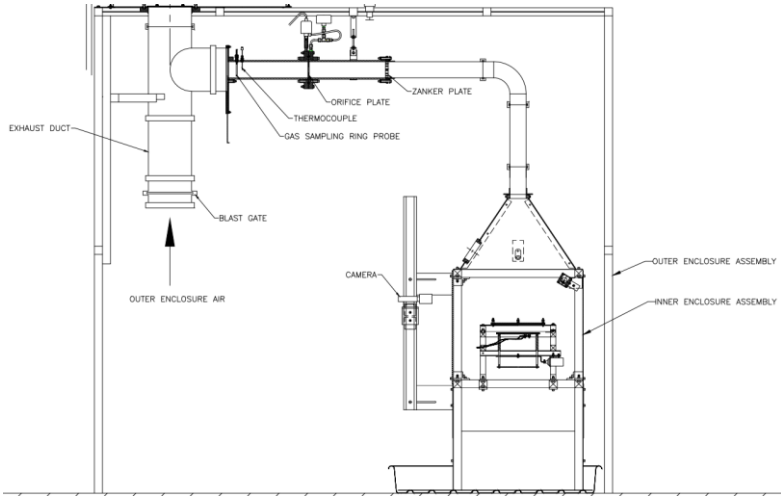

Figure 1. Schematic of outer and inner enclosures.

A. Experimental Enclosures

The experiment setup is shown in Figure 1. The outer and inner enclosures provide two levels of containment for the experiment products. The outer enclosure plumbs directly to the room ventilation, drawing room air from a gap around the perimeter of the enclosure between the enclosure walls and the floor. This creates a vented volume for the inner enclosure, which contains the battery under test, as well as measurement devices, in particular devices that vent through the case after performing measurements on product samples. A blast gate at the ventilation entrance controls the ratio of ventilation directly to the outer enclosure and through the inner enclosure and measurement duct. This outer enclosure is 2.44 m (8 ft) square, 2.29 m tall (7.5 ft), with a volume of 13.59 m^3 (480 ft^3). Three walls and the ceiling are aluminum sheets, with a front wall of polycarbonate doors for visibility during the experiment.

The inner enclosure contains the test article and is plumbed to the room ventilation via the measurement test section, described later. A gap between the floor and the walls of this enclosure allows make up room air to be pulled from the outer enclosure. The test section is 0.61 m (2 ft) square cross-section, 1.22 m (4 ft) tall, with a volume of 0.45 m^3 (16 ft^3). Two full orthogonal walls and the lower half of the other two walls are aluminum sheets, while the upper half of these two walls are removable polycarbonate windows for access and camera views. A 0.36 m (14 in) tall section transitions from the square cross-section of the enclosure to a 76 mm (3 in) diameter duct. A 0.42 m (16.5 in) duct and elbow connect the inner enclosure to the flow measurement duct. Two video cameras record orthogonal side views of the battery tests through the removable polycarbonate windows of the inner enclosure, while a third camera records the test from above through a window in the converging section of the inner enclosure.

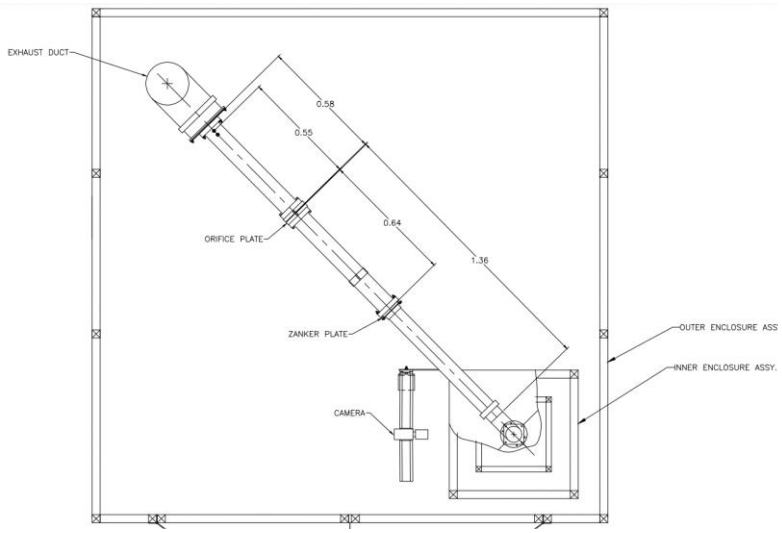

Figure 2. Drawing of flow measurement duct. Dimensions are in meters.

B. Data Measurement

Measurement of mass flow rate is a critical parameter for estimating heat released in open flow systems. In the current and planned tests of LIB thermal runaway, this is particularly true, as stages of the battery failure can produce more or less product gas, and future work with battery packs and laptops will also introduce temporal mass flow changes as materials adjacent to a failing battery begin to burn at different times during a test. This section describes the mass flow measurement duct, which connects the inner enclosure to the room ventilation described in the previous section. It also discusses two devices used to measure the concentration of oxygen, carbon dioxide, and carbon monoxide in the product stream.

The measurement duct, shown in Figure 2, is designed and built to ISO Standard 5167, describing flow measurement using pressure differential in circular cross-section ducts[12, 13]. Specifically, this system uses an orifice plate to develop the pressure differential. The duct is 76 mm (3 in) diameter galvanized steel. The duct is 1.35 m (53 in) long upstream to the orifice plate. A Zanker conditioning plate[13] is 0.62 m (24 in) upstream of the orifice plate. The conditioning plate reduces the required length of the upstream section from 23 duct diameters to 17[13]; this upstream section is 17.7 diameters long. The orifice plate used here is stainless steel, with an orifice 47.6 mm (1.875 in) in diameter. A Setra Systems (Boxborough, Massachusetts) Model ASL differential pressure sensor measures the change in pressure across the orifice plate, while a Setra Systems Model 204 static pressure sensor measures the static pressure on the upstream side of the orifice plate. The length of the duct downstream of the orifice plate is 0.5 m (19.6 in) long, or 6.6 pipe diameters; the minimum required length is 6 diameters[13]. The first penetrations of the measurement duct occur downstream of the final length and include a Type K thermocouple to measure gas stream temperature and a gas sampling ring for product gas measurement. The methods and equations of this ISO standard allow for real-time calculation of mass flow rate, and the static pressure and temperature measurements, with the assumption that the medium is isentropic perfect air, allow calculation of standard and actual volumetric flow rate[12, 13]. The maximum flow rate as currently configured is 2.12 standard* m^3/min (75 standard ft^3/min).

The system uses two measurement devices to determine the oxygen, carbon dioxide, and carbon monoxide in the gas stream. Both devices use their own pump to draw a sample of gas through the measurement duct sampling ring and a tee fitting, where the flow splits to the instruments. Upstream of this split is a HEPA filter (Pall Life Sciences Part Number 12144) and a water/ice cold trap to filter particulate and condense out volatile species before concentration measurement. The first device is a commercial Testo 350[14] (Testo, Inc., West Chester, PA), using

* Standard conditions are one atmosphere pressure, 21 °C (70 °F).

electrochemical sensors for O_2 in the range of 0-25%-vol and CO in the range of 0-10,000 ppm-vol, and for CO_2 a non-dispersive infrared (NDIR) sensor in the range of 6,000-500,000 ppm-vol. This system records data at 1 Hz. The second device is a reduced version of a laser absorption spectrometer custom-built at the NASA Jet Propulsion Lab, intended to monitor combustion products in the larger volume of a space vehicle or habitat[†15]. It reports O_2 concentrations between 15 and 45 %-vol, CO_2 between 300 and 30,000 ppm-vol, and CO between 5 and 1000 ppm-vol, with all measurements at 30 Hz via a data acquisition system described next. Testing with this device revealed that it is susceptible to aerosol interfering with the measurement. This is true even with a HEPA filter installed upstream of the device.

The data acquisition system uses a National Instruments (National Instruments, Austin, Texas) cDAQ-9178 backplane with two modules, a 9152 for voltage data acquisition and a 9214 for Type K thermocouple data acquisition. Additional voltage signals are recorded using a National Instruments USB-6003 at 400 Hz. The voltage system acquires data at 400 Hz for static and differential pressure, humidity, cell voltage, and gas concentration. The thermocouple temperatures are acquired at a hardware-limited 4 Hz; this is also the limit for reported flow rates and heat release rates, as these estimates require temperature measurements. The thermocouples measure cell temperature at multiple locations, plume temperature, and air and product flow temperature. Voltage data used in calculating flow and heat release rates averages 100 data points, reducing the effective sampling rate to 4 Hz corresponding with thermocouple data.

The LIB thermal runaway tests also included particle size distribution measurements using an Electrical Low-Pressure Impactor, ELPI+ (Dekati Ltd., Kangasala, Finland). The ELPI+ is a first principles particle size and charge distribution device, using a cascade impactor where charged aerosol particles deposit on one of 14 plates. The cumulative charge on each plate is a function of the particle mobility diameter, which is itself a function of particle size, morphology, density, and shape factor. The charges on each plate represent the sampled aerosol's particle size distribution. The ELPI+ reports these size distributions at 1 Hz, allowing for good temporal resolution. The aerosol is sampled through a 12.5 mm (0.5 in) diameter tube 300 mm (12 in) above the battery under test. Aerosol samples are drawn through the sampling tube and ELPI+ by a pump downstream of the device. The sample also has air dilution with a HEPA filter (Pall Life Sciences Part Number 12144), manually applied when necessary at a ratio of up to 4.2:1 to decrease particle concentration entering the instrument[16].

C. Oxygen Consumption Calorimetry

Heat release rate is one of the estimates of interest for lithium-ion battery thermal runaway, particularly in the context of crewed space vehicles and habitats. Many of the design choices made in building this apparatus, particularly the flow rate measurement duct, were made with a heat release estimate in mind. For this system, with continuously vented room air flowing through, oxygen consumption calorimetry provides the best method for these estimates. The equations used here are based on Janssens[17-19], using the equations and process of Chow and Han[20]. This process uses the mass flow rate and incoming and outflowing O_2, CO_2, and CO concentrations. Alternate equations allow for only the use of O_2 concentration instead of all three species. The use of O_2-only methods became necessary when even the HEPA filter and cold trap did not sufficiently remove aerosol and other contaminants with tests using one of the types of LIB described later.

Oxygen consumption calorimetry calculations also depend on a parameter, E, describing the amount of energy released per mass of oxygen consumed. For the ethanol pool testing, these calculations used a value of 13.3 MJ/kg-O_2 consumed[19], a value generally applicable to alcohols. Later testing with LIB used a value of 13.1 MJ/kg-O_2 consumed, a value generally used for complex fuels or fuels without previous characterization[19]. The total energy released is found using a trapezoidal numerical integration of the heat release rate[21].

D. Ethanol Pool Test Setup

The first test series of this containment and measurement system used a pan of burning ethanol as a heat source. One of two pans is used in each test, the first 100 mm (4 in) diameter and the second 200 mm (8 in) diameter. Both pans are 19 mm (0.75 in) deep. The 100 mm pan simulates a test with a single LIB, while the 200 mm pan simulates a larger battery pack test. Each pan is filled with 3 mm diameter glass beads to reduce the volume of liquid fuel. Before each test ethanol is added to the pan such that the liquid level reaches the rim of the pan, typically 50 ml for the dry 100 mm pan and 300 ml for the dry 200 mm pan. The test pan rests on a scale within the inner enclosure (Ohaus Corporation Ranger 7000), with data recorded at 10 Hz. All tests used room air flow at 1.42 m^3/min (50 ft^3/min), as the duct flow meter indicated. The test begins with the ethanol ignited by a long butane lighter, with the inner enclosure

[†] The version used here measures only O_2, CO_2, and CO; the standard model measures additional species.

access window immediately closed. The flame burns for five minutes, during which the scale measures fuel loss, the flow meter pressure and temperature measurements yield mass flow rate, and gas species are monitored. The video also records the event. After five minutes, test personnel open the access window and place a large aluminum plate over the pan to extinguish the flame.

The data analysis compared the results from two methods for estimating heat release rate. The first is the oxygen consumption calorimetry described in Section II.C. The second used a linear curve fit of the mass data during combustion (i.e. the mass loss rate of the ethanol), and multiplied that by the heat of combustion, H_c[22], 25.6 MJ/kg-ethanol. Both mass loss rate and heat of combustion are adjusted to reflect the mass of oxygen rather than fuel consumed. The linear fit of fuel mass loss and the published value of H_c are multiplied by the ratio of fuel to oxygen molecular weight and by the stoichiometric ratio of moles of fuel consumed to moles of oxygen consumed, 1:3 in the case of ethanol. The adjusted H_c is 12.3 MJ/kg-O_2 consumed, somewhat smaller than the 13.1 MJ/kg-O_2 consumed described in the previous oxygen consumption calorimetry section for alcohols.

E. Battery Test Setup

The experiments described here focus on the thermal runaway of two single-cell prismatic batteries, an AA Portable Power Corporation model 544792 ("AA") and KULR Technology M281 ("KULR"). The AA battery is a lithium cobalt oxide cell, while the KULR is a cobalt lithium manganese nickel cell. Both types are 2500 mAh, 3.7 VDC devices, fully charged for the test. Figure 3 shows a schematic of the typical battery setup for a test intended to mimic a battery cell in a battery pack. The top and bottom layers are sheets of flame retardant garolite, a glass fiber board used in circuit boards. Above and below the battery are layers of glass fiber insulation. Springs on mounting posts provide compression on the battery and insulation stack, again mimicking the conditions for a battery in a battery pack. Six Type K thermocouples provide surface temperature measurements of the battery during the test, with three on each face of the battery, one near the terminals, one near the center, and a third at the end. Four additional Type K thermocouples between the fiber insulation and the plate and on the outer surface of the plate, the top and bottom of the battery provide additional temperature measurements during the test process. A final thermocouple is placed above the electrodes to measure gas escaping from this typically weak point in the battery packaging. All thermocouples have bare wire, 0.25 mm diameter beads.

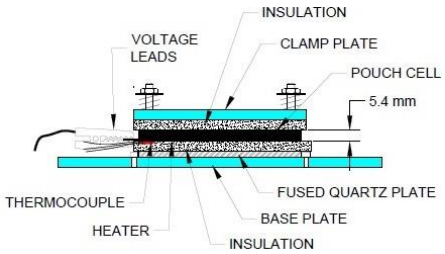

Figure 3. Drawing of lithium-ion battery test setup, with insulation, mounting plates, thermocouples, and heater shown.

A surface heater (DwyerOmega Instruments Model KHA 304/10), 10 W/in^2 power and the same size as the battery (7.62 cm by 10.16 cm) heats the battery to thermal runaway. Heater power is controlled by a PID controller (Watlow Electric Manufacturing Company Model F4T), with a thermocouple at the center of the battery cell bottom face providing the feedback temperature. The controller follows a ramp and soak profile, where temperature increases linearly from room temperature (typically 20-22 °C) to 250 °C in 10 minutes, holding that temperature for 5 minutes, then increasing from 250 °C to 300 °C in 5 minutes, then holding temperature until disabled. It is important to note that the PID algorithm will not enable the heaters once TR begins. As later sections show, the battery reaches a temperature of 800 °C when thermal runaway begins. This is much larger than the ramp and soak set points described, and the PID algorithm will not apply power if the battery feedback temperature is larger than the set point. Additionally, operators disable the heater soon after the thermal runaway begins.

III. Ethanol Pool Results

Table 1. Peak heat release rates of four ethanol pool tests, compared with estimates based on mass loss and consumption of O_2.

Test Number	Pan Diameter (mm)	Three Species Calorimetry (kW)	O_2-Only Calorimetry (kW)	Rate of Mass Loss Estimate (kW)
1	100	1.66	1.84	1.67
2	100	1.52	1.70	1.73
3	200	9.04	9.88	10.78
4	200	9.40	10.23	11.21

This section reports the results of four representative ethanol pool burning tests, two each of 100 mm and 200 mm pools. As discussed in the previous section, the 100 mm ethanol pool tests are roughly representative of individual battery cell thermal runaway tests, while 200 mm pool tests are roughly representative of larger laptop battery packs or full laptop computer thermal runaway tests. Table 1 presents the heat release rate results, with calorimetry calculated using all three species as well as oxygen alone. The third column shows the expected heat released based on the linear fit of fuel mass loss and heat of combustion, re-scaled to reflect oxygen rather than fuel loss. For the 100 mm pans, the calorimetry estimates heat release between 1.52 and 1.66 kW with all three species and 1.70 to 1.84 kW for calculations using only oxygen concentration. The corresponding heat release rate estimates based on heat of combustion range from 1.67 to 1.73 kW. These results show that the agreement between the three species and the O_2-only methods of calorimetry is within 10%, and the calorimetry methods agree within 20% of the heat of combustion calculations. Figure 4a shows these results graphically for Test 1. The 200 mm pan tests show similar results. The calorimetry heat release estimates range from 9.04 to 9.40 kW for calculations using all three species and 9.88 to 10.23 kW for O_2 only calculations. The corresponding heat release estimates based on heat of combustion range from 10.78 to 11.22 kW. These results also show agreement between the two calorimetry calculations of 10%, while the agreement between the calorimetry and heat of combustion estimates vary more for these larger pan tests, in the range of 20%. Figure 4c shows these results graphically for Test 3. Overall, the good agreement between the calorimetry and heat of combustion estimates of heat release rate show that the apparatus performs well in containing

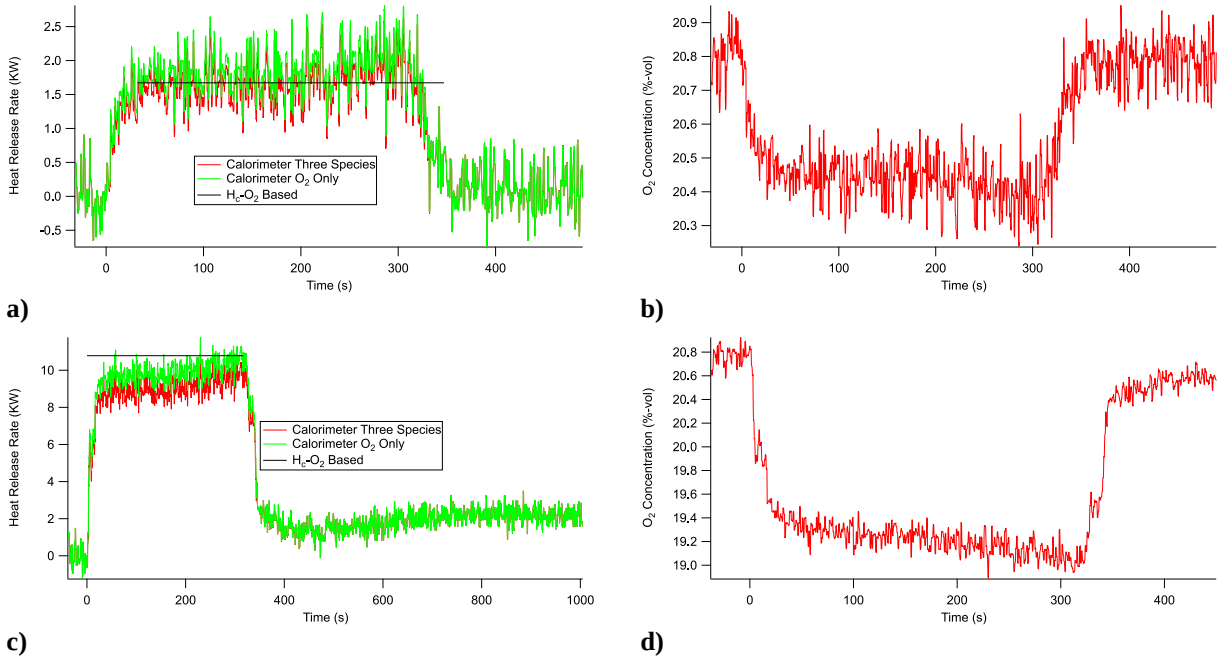

Figure 4. Heat release rates and oxygen concentrations for a 100 mm and a 200 mm ethanol pool fire. *Graphs a) and b) are from a 100 mm pool fire (Test 1), while graphs c) and d) are from a 200 mm pool fire (Test 3). Ignition is at time 0 seconds.*

a fire event and providing data on flow rate, pressure, temperature, and gas concentration to make heat release estimates from the event.

These tests are also useful for determining the amount of oxygen consumed by fires of different sizes for the given induced flow rate of 1.42 m^3/min. Figure 4b and 4d show the oxygen concentration in a 100 mm pan (Test 1), and for a 200 mm pan (Test 3), respectively. Test 1 shows a decrease in oxygen concentration from 20.8 %-vol to 20.4 %-vol, while Test 3 showed a decrease from 20.8 %-vol to 19.4 %-vol, with the concentration further decreasing gradually over the five-minute test to 19.0 %-vol. These results show that the resolution and accuracy of the oxygen sensor must be balanced against the flow rate, such that sufficient room air flows in to sustain the combustion while providing enough oxygen loss to the outlet for sufficient measurement and will be a consideration for all future testing with this apparatus.

IV. Lithium-Ion Battery Cell Results

The second series of tests focuses on two manufacturers of lithium-ion batteries (LIBs), with similar characteristics but different results. This discussion focuses first on the AA Portable Power (AA) battery tests, then the KULR tests, followed by a comparison of the results.

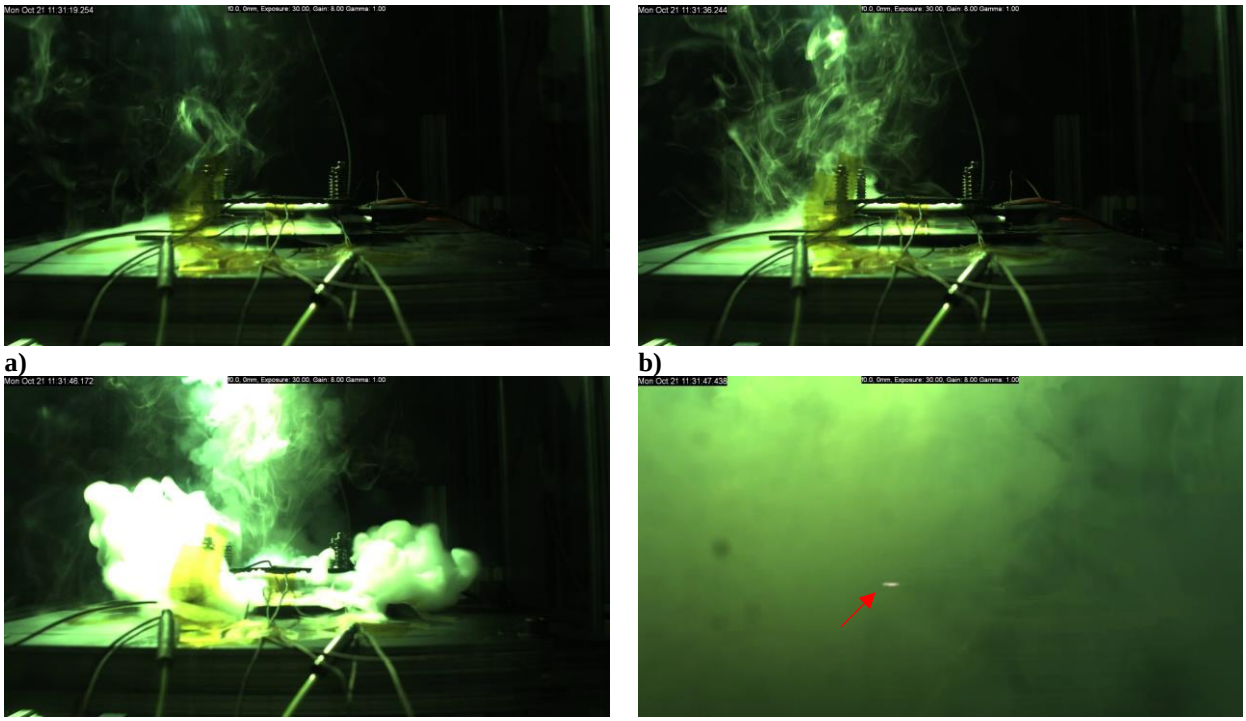

Figure 5. A sequence of images showing the process leading to thermal runaway for an AA LIB. *Figure a) shows the accumulation of heavier than air aerosol, white wisps on the black garolite background, along with some whisps of lighter aerosol 11 minutes into heating. Figure b) shows the transition to mostly lighter than air aerosol 12 minutes into heating. Figure c) depicts the onset of thermal runaway, 11.5 minutes into heating, marked by a significant release of aerosol. Figure d) shows the small traces of flame or incandescing material in the battery (noted by the red arrow), with the test volume filled with aerosol, one second after thermal runaway begins.*

A. AA Battery Test Results

Figure 5 shows a series of images from a representative AA battery test. In all cases, time = 0 seconds is when the heating ramp began. Figure 5a shows the accumulation of heavier-than-air aerosol and combustion products around the battery, visible as wisps of white on the black garolite base, after 11 minutes of heating. One minute later, additional aerosol and gas, lighter than air, form plumes above the battery, as shown in Figure 5b. Thirty seconds later, the battery enters TR, emitting a large amount of gas and aerosol, as seen in Figure 5c. One second later, the volume of the inner enclosure is filled with aerosol and gas products, obscuring the objects within, as shown in Figure 5d. A small glowing

region of the battery can be seen as well, noted by the red arrow. It is suspected that this is a small region where electrolyte or other battery components are burning. Another possibility is the region of the battery is hot enough to incandesce. Figures 5c and d also show that the plumes of aerosol and ejected material extend far from the test cell. This shows the necessity for building the inner enclosure as large as possible, to contain and capture the gas products and aerosol to the largest extent possible for both user safety as well as quantifying these products for evaluation of vehicle fire safety impacts. This result demonstrates the infeasibility of a commercial cone calorimeter.

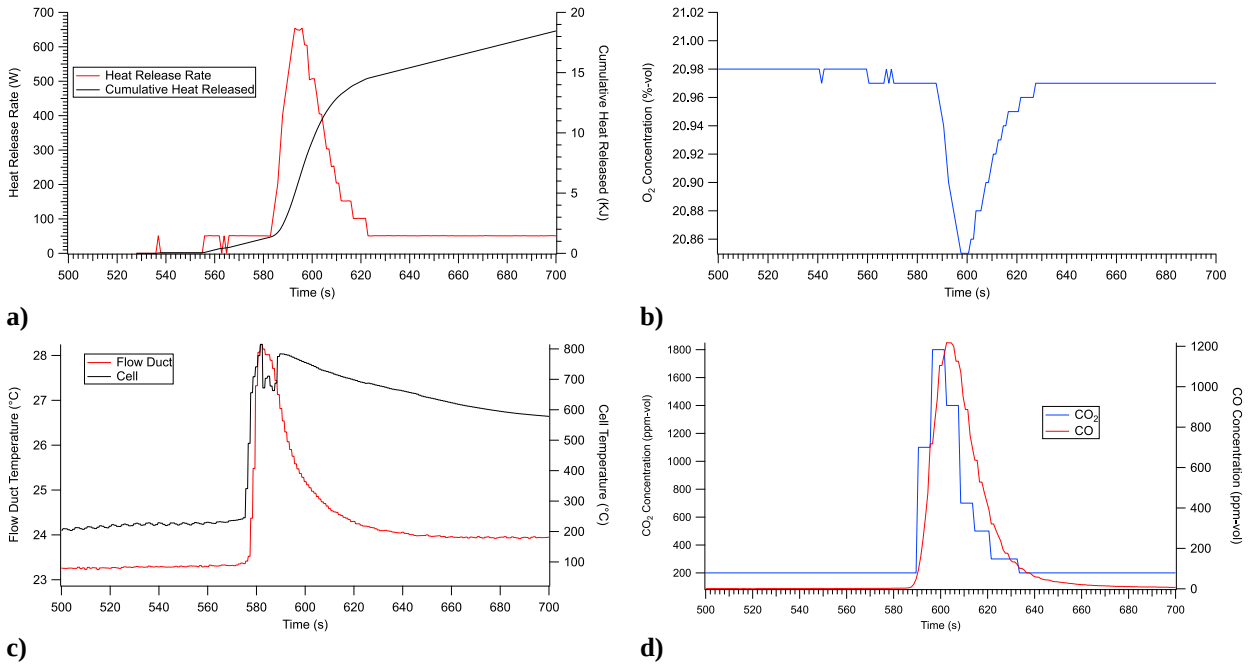

Figure 6. Results from a representative AA LIB in thermal runaway. *a) Heat release rate (left axis) and cumulative heat released (right axis) during thermal runaway. b) O_2 concentration, used to estimate heat release rate. c) Temperature of air and product stream in the measurement duct and the temperature of the LIB. d) CO_2 and CO concentration during thermal runaway. Time 0 seconds is beginning of heating.*

Figure 6 shows presents data collected from this representative AA battery thermal runaway test. Figure 6a shows the heat release rate in Watts (left axis) and the cumulative heat released in kilojoules (right axis) during TR. The heat release rate peaks at 650 W, with a cumulative heat released of 18 kJ. The rise in heat release is consistent with the observation of the small flame or glowing region of the battery during the test. The oxygen concentration is shown in Figure 6b, with a small deflection (0.2%-vol) during TR, and steady concentration at room air values (~20.9 %-vol) before and after TR. The cell temperature and air temperature in the measurement duct are shown in Figure 6c. These data show a sudden increase in cell temperature at TR, from 250 °C to 800 °C in two seconds. The flow duct air temperature also rises sharply as hot products from TR mix with the air, from 23 °C to 28 °C. Finally, Figure 6d shows the CO_2 and CO concentration during TR. The failing battery emits these product gases during TR, with concentrations at background levels both before and after the TR event. The event also produced large amounts of CO_2 and CO. The CO_2 concentration rises from a room level of 500 ppm-vol to over 1600 ppm-vol, while the CO rises from 0 ppm-vol to 1200 ppm-vol. The concentration of CO is particularly noteworthy, as the amount produced could pose a toxicity risk to nearby personnel in enclosed or poorly ventilated areas.

These tests also produced particle concentration and size distribution results, with this representative case shown in Figure . Figure 7a shows the total number concentration ("PN10," number of particles per cm^3 sampled air) over the entire course of the test, from the beginning of heating through TR and afterward. Because of the dynamic concentrations generated by battery tests and limitations to the ELPI+ analyzable concentration ranges, aerosol dilution was applied as needed, as represented in 7a. Here, the dilution factor, "DF," is equal to the ratio of the total ELPI+ flow rate (Q_{total}) to the aerosol sample flow rate ($Q_{total} - Q_{dilution}$). Figure 7b presents the size distribution of the particles during these three phases, with the colors corresponding to the time indicated in Figure 7a.

In the early stages, the battery releases low concentrations of small particles, with diameters of 10s of nm, as indicated by the light blue line. This particle emission coincides with low heater temperatures, resulting from

volatilization and nucleation of external battery components, material on the heater, or both. As TR approaches, the battery begins releasing more aerosol, and the mode of the aerosol diameters shifts to larger diameters, shown by the purple line. At the onset of TR (dark red line), just before introduction of dilution, the aerosol becomes bimodal, with particle diameters in the order of 10 nm and a second mode near 100 nm. After TR, the particle size distribution shifts to a mode around 30 nm, represented by the red line.

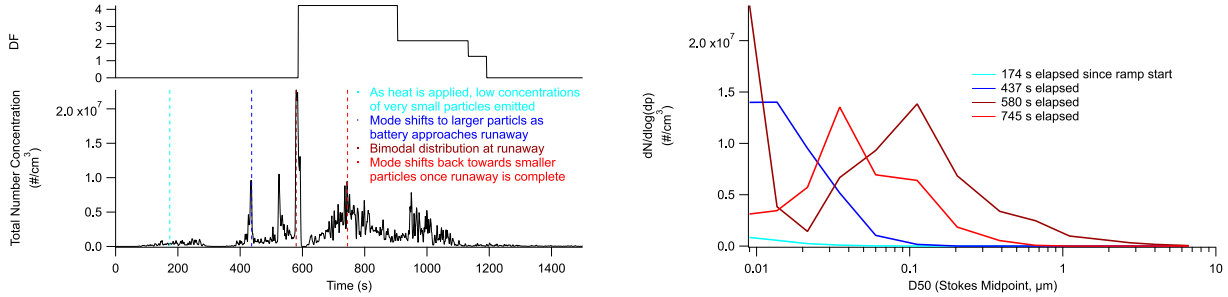

a) **b)**

Figure 7. Aerosol number concentration (left) and size distribution (right) for an AA battery test. *a) shows Number concentration of particles at different phases of the test, from the beginning of heating through TR and cooling, as well as the dilution factor (DF). Dilution (~3.5/1) applied at 600 s to preserve the instrument at high particle concentrations, with the dilution slowly ramped down between 700 and 800 seconds to capture more features in particle concentration. b) Size distribution during heating, near thermal runaway, at thermal runaway, and during cooling.*

B. KULR Battery Test Results

Figure 6 shows a sequence of images from a representative KULR battery test to a thermal runaway. As with the AA cell tests, the heating ramp began at a time of 0 seconds. Figure 6a shows the battery 9 minutes into heating, where buoyant plumes of aerosol can be seen. Unlike the previous AA LIB tests, there is no heavier-than-air aerosol or products pooling around the battery. Figure 6b, 10 seconds later, shows a jet of aerosol exiting the battery at the thermal runaway. Figure 6c, one second later, shows the early stages of sparks and glowing debris ejected from the battery. A quarter-second later, Figure 6d shows the ignition of this plume, developing into a flame jet 1/30 of a second later in Figure 6e. Subsequent images saturate the camera as flame engulfs the battery. The flames recede, as shown in Figure 6f 4 seconds after Figure 6e, where the battery is still on fire. As with the previous AA cell test, the results of this test show the need for a large enclosure, larger than a commercial cone calorimeter, to contain and capture for analysis the aerosol and gas products of a lithium-ion battery fire during thermal runaway.

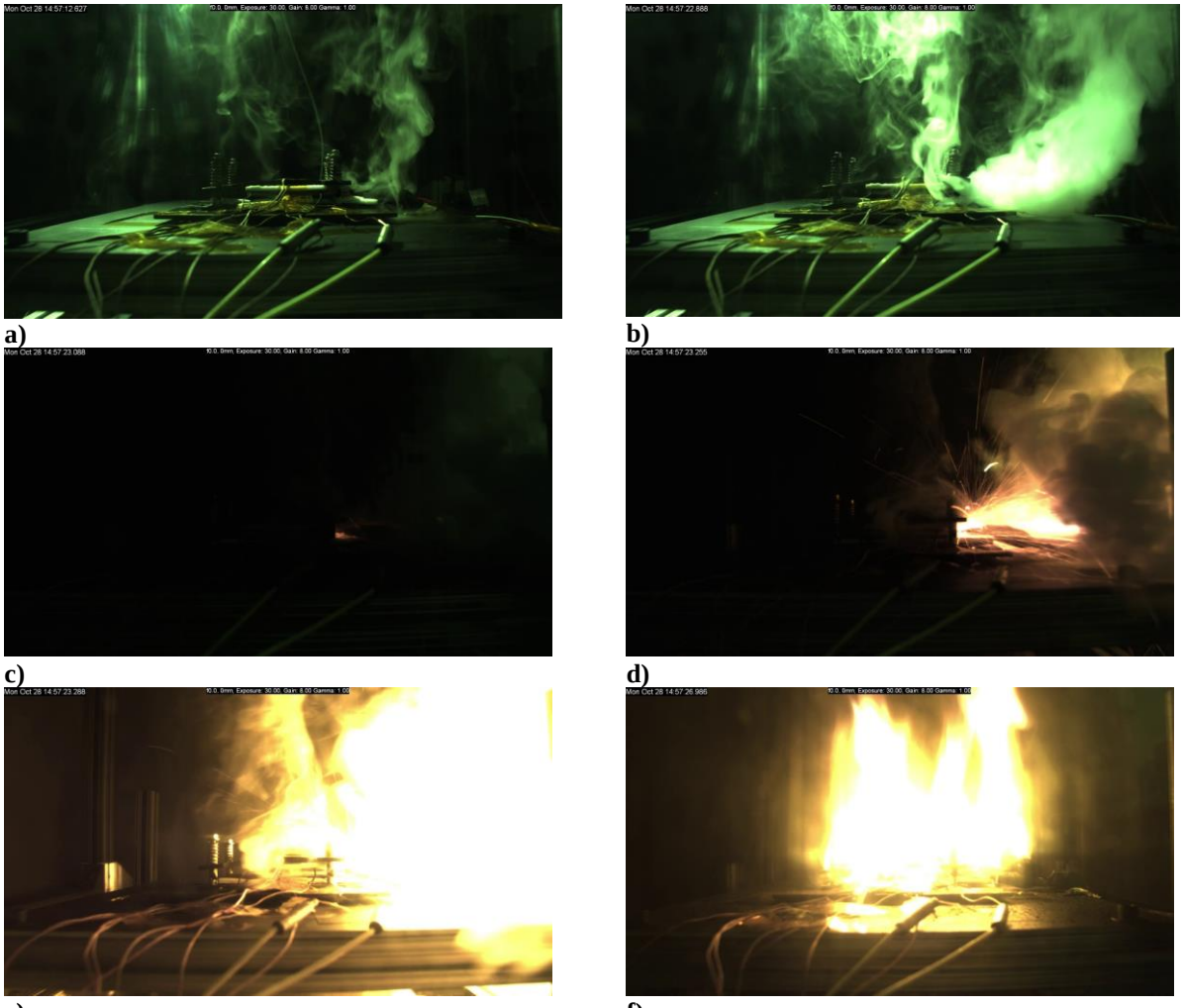

Figure 6. A sequence of images showing the process leading to thermal runaway for a KULR LIB. *Image a) shows the battery 9 minutes into heating with buoyant aerosol plumes but no heavier-than-air material. Image b) is 30 seconds later, showing a large plume of aerosol ejected from the battery near the terminals at TR. Image c) is one second later, showing early stages of incandescing material ejected from the cell. Image d) is 0.25 seconds later, showing extensive ejected material and the beginning of flames. Image e) 0.030 seconds later, showing extensive flames saturating the camera. Image f) is 4 seconds later, after jetting flames have ended but the battery is burning with flames visible. Most of the images between images e) and f) are saturated.*

Figure 7 presents data from this TR test. Figure 7a shows that the peak heat release rate is 5 kW during TR, with a cumulative heat released of 80 kJ, significantly larger than those obtained in the AA test. These results are consistent

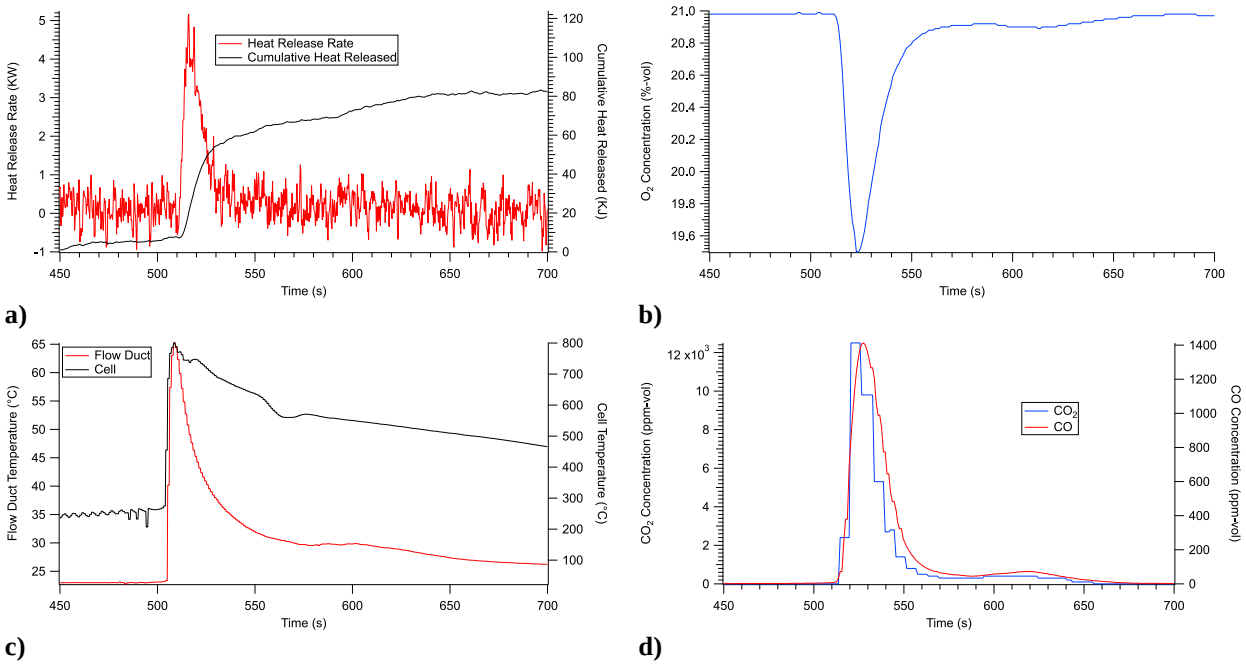

Figure 7. Results from a representative Kulr LIB. *Figure a) shows the heat release rate (left) and cumulative heat released (right) during thermal runaway. Figure b) shows the oxygen concentration, used to estimate heat release rate. Figure c) shows the temperature of air and product stream in the measurement duct and the temperature of the LIB, and figure d) shows the CO_2 and CO concentration during thermal runaway. Time 0 seconds is the beginning of heating.*

with the large jet of flame and engulfed battery during thermal runaway. Figure 7b shows that the oxygen concentration dropped from 20.9 to 19.5 %-volume during TR. The O2 concentration returned to background values approximately thirty seconds after TR ended. Again, this larger oxygen consumption is consistent with the large flames seen in this test. In Figure 7c the flow temperature and the temperature of the LIB surface temperature show large, sudden increases, with the measurement duct temperature rising from room temperature to 65 °C, and the LIB cell temperature rising from 250 °C to 800 °C in one second. The increase in temperature corresponds with the increase in heat released during this test. Despite the different phenomena and heat release, the LIB cell temperature corresponding with the AA test shows that the flame and heat release seen here point to differences in the electrolyte used, while phenomena internal to the battery are similar in these cases. In Figure 7d, the CO_2 concentration rises from a room value of 500 ppm-vol to more than 12000 ppm-vol, while the CO reaches a peak of 1400 ppm-vol during thermal runaway. This shows the effect of both the decomposition and burning of the electrolyte in this case and the toxic conditions that can arise from a LIB in thermal runaway.

While these tests included aerosol sampling and measurements, the results are inconclusive. The battery did not produce significant amounts of aerosol leading up to TR, making measurements difficult. Further, the TR event produced significant flame, but the flame jets pointed away from the sampling port and impinged on the inner enclosure window. These factors complicated aerosol sampling and data interpretation in the current configuration and will be addressed in future work.

C. Comparison of Different Lithium-Ion Battery Results

These initial results show the differences between lithium-ion batteries in thermal runaway despite the battery cells having similar performance characteristics and use cases. The AA batteries weak or no visible combustion during TR, released minimal heat, and instead produce large quantities of aerosol, CO_2, and CO. In contrast, the KULR batteries, by contrast, produced large flames and heat release, as well as CO_2 and CO. These batteries also produced significantly less aerosol while producing large soot particles and other ejected material. These differences highlight that batteries, with varying cell chemistries, can produce vastly different outcomes during thermal runaway. The associated risks and threats posed by these differences, as well as the detection and countermeasure devices and plans for them, must be considered by mission planners and vehicle system designers. Batteries in thermal runaway may produce a range

of phenomena, and planning for one type of response may leave unacceptable risk when a different cell type is used by a manufacturer, possibly without the knowledge of the vehicle and mission planners. One similarity between the two battery types during thermal runaway is the cell temperature. In both cases, the temperature rose to approximately the same level, 800 °C, within one to two seconds of the onset of thermal runaway. This highlights an additional risk posed by batteries in TR, they can act as a heat source capable of igniting surrounding material.

The present AA LIB results also show a difference from published results using the same cell, though with a different method of inducing TR[5, 6]. The present work used a flexible surface heater following a set ramp and soak prescription, with the heating ending at thermal runaway because the feedback temperature, the surface of the battery cell, was higher than the set point temperature. The previous work used a temperature-controlled hot plate to heat the LIB to thermal runaway, but the plate was temperature-controlled; battery temperature played no part in the control loop. In this work, the battery produced a large amount of aerosol but very little flame, while the previous work described the battery in flames; in fact, the hot plate in the previous work was not disabled until the flames self-extinguished. This points out another aspect of thermal runaway studies, which is that the method of inducing thermal runaway can itself effect the phenomena of thermal runaway[9]. This also implicates the types of scenarios that must be planned to protect vehicles and crews.

V. Conclusion

As part of an effort to quantify the risks to a space vehicle and crew during a lithium-ion battery fire and thermal runaway, the authors built a room-air vented enclosure with two levels of containment. The inner enclosure is sized for test articles ranging from 2500 mAh battery cells to laptop battery packs and tablet and laptop computers. It will capture aerosol and gas products for analysis. This enclosure vents through an orifice plate flow measurement system and gas concentration sensors provide information on CO_2 and CO produced, oxygen consumed, and heat released, based on oxygen consumption calorimetry, during the thermal runaway event. Initial validation testing with pools of ethanol showed reasonable agreement between heat released based on oxygen consumption and mass loss during burning. Initial tests with the two different LIBs, each 2500 mAh, showed different thermal runaway phenomena, where one type released considerable amounts of aerosol with little heat release while the other produced a small amount of aerosol but considerable heat release, flame jets, and burning material. Compared with other researchers, one of the batteries in this test only produced aerosol, while the previous work found flames with batteries of the same type from the same manufacturer. These results also show the need for a larger containment system, as aerosol and flame plumes were much larger than could be contained by a commercial cone calorimeter. Further testing with these types of batteries will confirm these results. These initial results show that the chemistry of the battery and method of thermal runaway may be important considerations for future experiments and fire safety planning for space vehicles and crew.

Acknowledgments

The authors would like to thank Dan Gotti, Universities Space Research Association, Cleveland, OH, for his work designing and building the inner enclosure and flow measurement duct, and the technicians at NASA Glenn Research Center, Cleveland, OH, for their work machining, assembling, and wiring various components of the apparatus. This work is funded through the Mars Campaign Office, NASA Marshall Space Flight Center, Huntsville, AL.

References

[1]Padilla, et al., “Hazardous Effects of Li-Ion Battery Based Fires,”, *2020 International Conference on Environmental Systems*, 31 July 2020.

[2]Padilla, R. E.., Dietrich, D. L., Pitz, W. J., Ruff, G. A., and Urban, D. L. “Battery Fire Risk Assessment,” *The 50th International Conference on Environmental Systems*, 12-14 July 2021.

[3]Urban, et al., “Preliminary Results from the Saffire VI Experiment”, *53rd International Conference On Environmental Systems*, 21-25 July 2024.

[4]Larsson, F., Andersson, P., Blomqvist, P., Loren, A. Mellander, B.-E., “Characteristics of Lithium-Ion Batteries During Fire Tests,” *Journal of Power Sources*, Vol. 271, December, 2014, pp 414-420.

[5]Classen,M., et al., “Characterization of Lithium-Ion Battery Fire Emissions-Part 1: Chemical Composition of Fine Particles ($PM_{2.5}$),” *Batteries,* Vol. 10, No. 10, 2024, pp. 301-324.

[6]Classen, M., et al., “Characterization of Lithium-Ion Battery Fire Emissions-Part 2: Particle Size Distributions and Emission Factors,” *Batteries,* Vol 10, No. 10, 2024, pp. 366-380.

[7]Sun, J., et al., “Toxicity, A Serious Concern of Thermal Runaway from Commercial Li-Ion Battery”, *Nano Energy*, Vol. 27, September, 2016, pp. 313-319.

[8]Yuan, L., Dubaniewicz, T., Zlochower, I., Thomas, R., and Rayyan, N., "Experimental Study on Thermal Runaway and Vented Gases of Lithium-Ion Cells," *Process Safety and Environmental Protection*, Vol. 144, December, 2020, pp. 186-192.

[9]Fernandes, Y., Bry, A., and de Persis, S., "Identification and Quantification of Gases Emitted During Abuse Tests By Overcharge Of A Commercial Li-Ion Battery," *Journal of Power Sources*, Vol. 389, June, 2018, pp. 106-119.

[10]Willstrand, O., Pushp, M., Andersson, P., and Brandell, D., "Impact of Different Li-Ion Cell Test Conditions on Thermal Runaway characteristics and Gas Release Measurements," *Journal of Energy Storage*, Vol. 68, September, 2023, pp. 107785.

[11]Willstrand, O., Pushp, M., Ingason, H., and Brandell, D., "Uncertainties in the use of oxygen consumption calorimetry for heat release measurements in lithium-ion battery fires," *Fire Safety Journal*, Vol 143, 2024.

[12]International Organization for Standardization, "Measurement of fluid flow by means of pressure differential devices inserted in circular cross-section conduits running full – Part 1: General principles and requirements," ISO 5167-1:2022(E), 2022.

[13]International Organization for Standardization, "Measurement of fluid flow by means of pressure differential devices inserted in circular cross-section conduits running full – Part 2: Orifice plates," ISO 5167-2:2022(E), 2022.

[14]https://www.testo.com/en-US/testo-350/p/0632-3510#tab-technicalData [cited 21 February 2025].

[15]Briggs, et al., "Five-Channel Infrared Laser Absorption Spectrometer for Combustion Product Monitoring Aboard Manned Spacecraft," *The 44th International Conference on Environmental Systems*, Tucson, AZ, 13-17 July 2014.

[16]A. Järvinen, M. Aitomaa, A. Rostedt, J. Keskinen, J. Yli-Ojanperä, "Calibration of the new electrical low pressure impactor (ELPI+)", *Journal of Aerosol Science*, Volume 69, 2014, pp. 150-159.

[17]Janssens, M. L., "Measuring Rate of Heat Release by Oxygen Consumption", *Fire Technology*, Volume 27, 1991, pp. 234-249.

[18]Janssens, M., "Heat Release Rate (HRR)", *Measurement Needs for Fire Safety: Proceedings of an International Workshop*, NISTIR 65237, edited by Ohlemiller, T. J., Johnsson, E. L., and Gann, R. G., National Institute of Standards and Technology, Gaithersburg, MD, 2000, pp. 186-206.

[19]Janssens, M., "Calorimetry," *The SFPE Handbook of Fire Protection Engineering, Third Edition*, The National Fire Protection Association, Quincy, MA, 2002, pp. 3-46 – 3-48.

[20]Chow, W. K., and Han, S. S., "Heat Release Rate Calculation in Oxygen Consumption Calorimetry," *Applied Thermal Engineering*, Vol. 31, Issues 2-3, 2011, pp. 304-310.

[21]Igor Pro 8, Software Package, Ver. 8.0.4.2, WaveMetrics, Inc., Lake Oswego, OR, 2019.

[22]Tewarson, A., "Generation of Heat and Chemical Compounds in Fires", *The SFPE Handbook of Fire Protection Engineering, 2nd Edition*, edited by DiNenno et al., National Fire Protection Association, Quincy, MA, 1995, pp. 3-53 – 3-124.